Supplimentary Material

Flexible MXene Nanosheet/Multiwall Carbon Nanotube-Reinforced Poly(vinylidene fluoride hexafluoropropylene)-Polymethyl Methacrylate Composites for Energy Storage and EMI Shielding

Nitesh Kumar Nath[a], Rajanikanta Parida[b], Bichitra Nanda Parida[c], Dibyaranjan Das[d],

S. K. S. Parashar[d], and Nimai C. Nayak*[a]

[a]Micro and Nano Materials Laboratory, Department of Chemistry, Faculty of Engg & Technology (ITER), Siksha'O'Anusandhan (Deemed to be University), Khandagiri Square, Bhubaneswar, Odisha-751030, India.

[b]Department of physics, Faculty of Engg & Technology (ITER), Siksha'O'Anusandhan (Deemed to be University), Khandagiri Square, Bhubaneswar, Odisha-751030, India.

[c]Central Institute of Technology, Kokrajhar (Deemed to be University, MHRD, Govt. of India) BTAD, Assam-783370, India

[d]Nanosensor Lab, School of Applied Sciences, Kalinga Institute of Industrial Technology (KIIT) Deemed to be University, Campus-3, Bhubaneswar, Odisha, 751024, India

**to whom correspondence should be made; nimainayak@soa.ac.in*

1. Mechanism of Conductive network Formation

The Figure S1 depicts the hybrid conductive network and polymer-filler interactions in the composite. The PVDF-HFP matrix provides a ferroelectric, polar environment rich in -CF_2 dipoles, while PMMA domains enhance blend compatibility and regulate dielectric loss through dipole-dipole interactions between PMMA carbonyl (C=O) groups and PVDF-HFP chains. MXene sheets**,** decorated with surface terminations (-O, -OH, -F), interact strongly with the polymer chains via hydrogen bonding and electrostatic interactions, ensuring good interfacial adhesion. MWCNTs, with their high aspect ratio, act as 1D conductive bridges between MXene sheets, suppressing MXene restacking and enabling the formation of a 3D percolative conductive network.

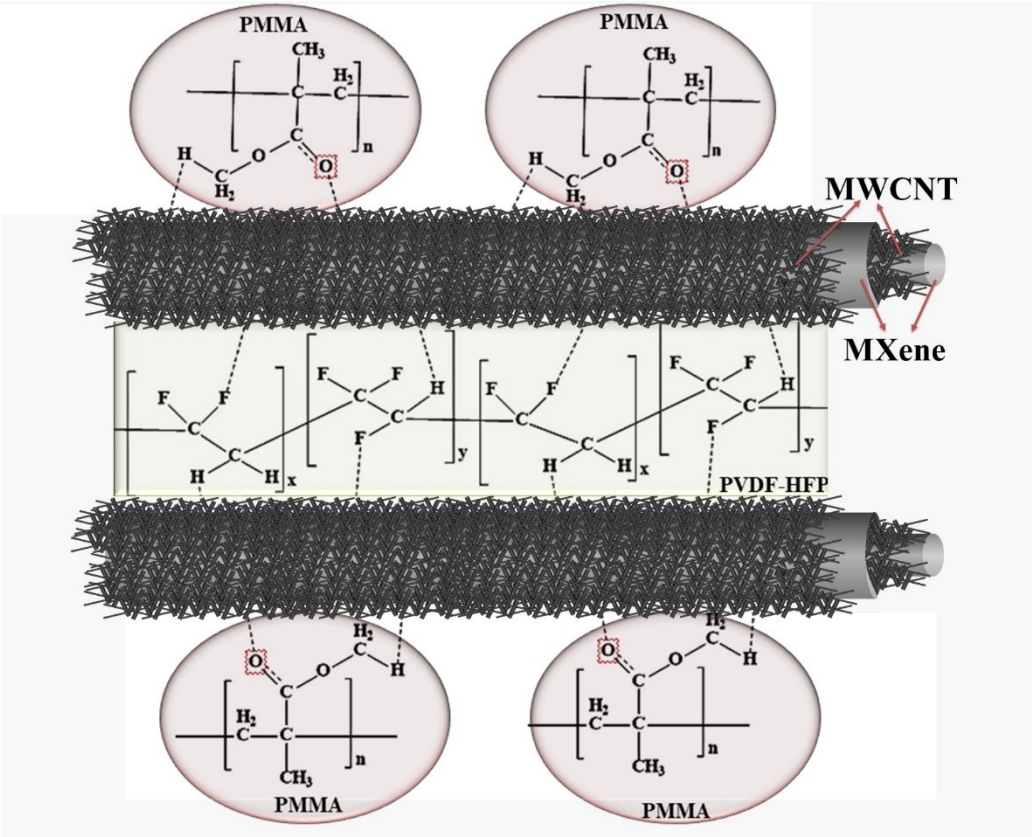

Figure S1. This schematic provides polymer-filler interactions which strengthens the mechanistic interpretation of the experimental results.

2. Functionalization of $Ti_3C_2T_x$ MXene & MWCNTs

The XRD, FT-IR and Raman patterns of $Ti_3C_2T_x$ MXenes are shown in Figure S2(a-c), respectively. In our earlier research, we had previously addressed the characteristics of MXene [1]. The new peaks were simultaneously found at 2θ of 8.9° and 18.5°, indicating that F had been added to the interlayer of MXenes. Additionally, a novel peak at 27.54° was found and identified as $Ti_3C_2(OH)_2$ [2]. In accordance with these results, the surfaces were modified with -OH and -F functional groups followed by HF etching. Broad absorption is facilitated by the stretching of O-H from surface functional groups at about 3446 cm^{-1}. There is a peak at about 1624 cm^{-1} (H-O-H bending), and bands at approximately 600-800 cm^{-1} reflect Ti-O and Ti-C vibrations. Strong peaks that represent Ti, C, and surface terminations are located between 200 and 800 cm^{-1}. There are noticeable peaks at approximately 271 cm^{-1} and 600 cm^{-1} that are related to Ti-C vibrations. Figure S2(d) displays surface images of as obtained pure $Ti_3C_2T_x$ MXenes. A comparable two-dimensional layered structure was developed by removing an Al atom from Ti_3AlC_2 after HF etching. The characteristics of f-MWCNTs are depicted in Figure S2(e-h). The XRD pattern, which displays the strongest peak at ~26.2° corresponding to C (002) planes, a characteristic of highly graphitic nature, has been used to demonstrate the structural phase of the MWCNTs. The absorption bands in FT-IR spectra are induced by the existence of C=O (1632 cm^{-1}), and O-H (3456 cm^{-1}). These are related to the presence of water adsorbed on the surface and hydroxyl groups created during the oxidation of nanotubes. The three primary characteristic bands of Raman spectra D (1354 cm^{-1}, symmetric), G (1588 cm^{-1}, asymmetric), and 2D (2650 cm^{-1}, symmetric), which confirm the formation of top-notch MWCNTs [3-4]. As depicted FESEM image, the tubes are several microns long and between 50-100 nm thickness. Additionally, MWCNTs are spherical structures with individual carbon nanotubes interconnected within themselves.

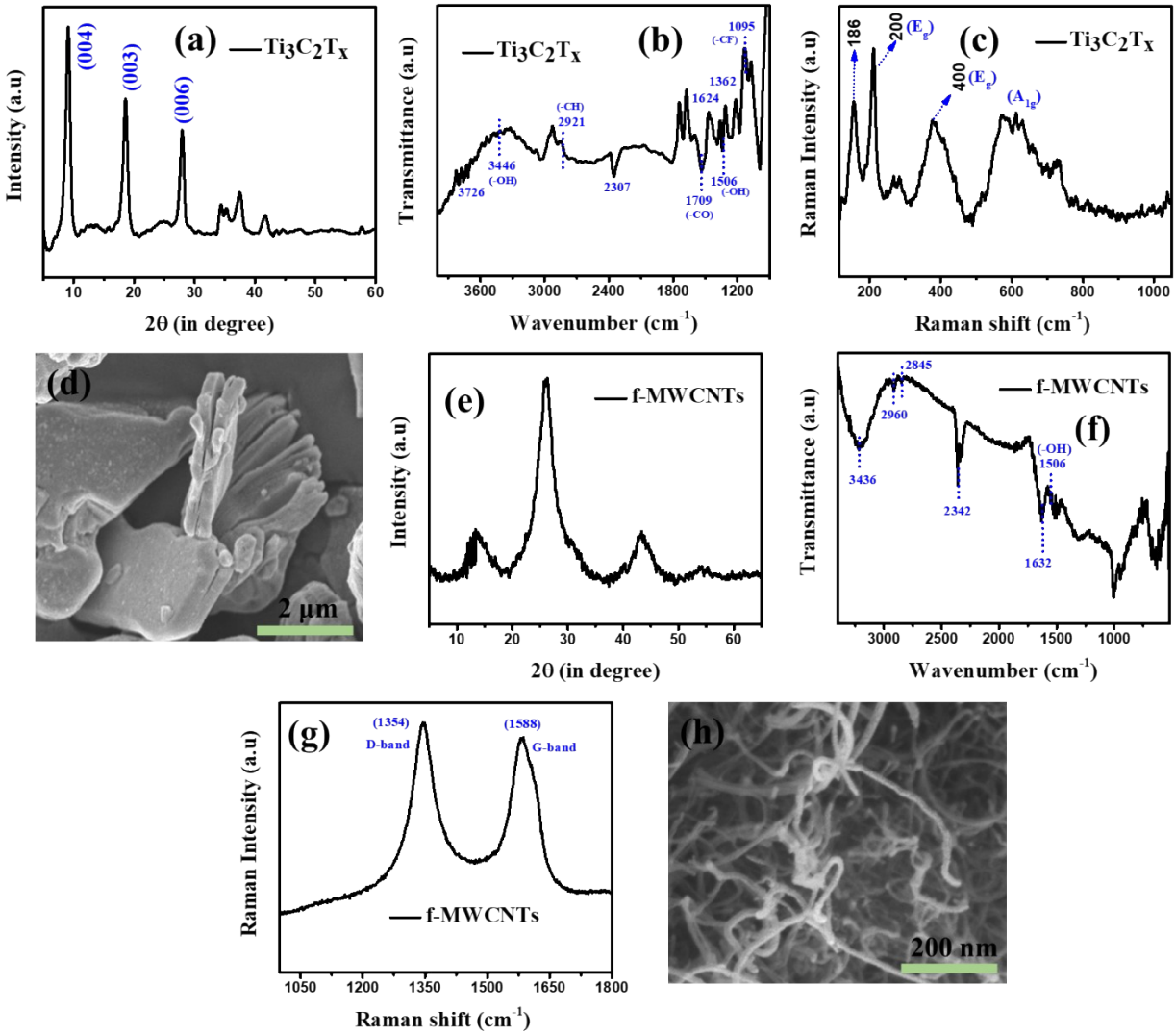

Figure S2. (a-d) XRD, FT-IR, Raman and FESEM of $Ti_3C_2T_x$ MXene, respectively (e-h) XRD, FT-IR, Raman and FESEM of f-MWCNTs, respectively.

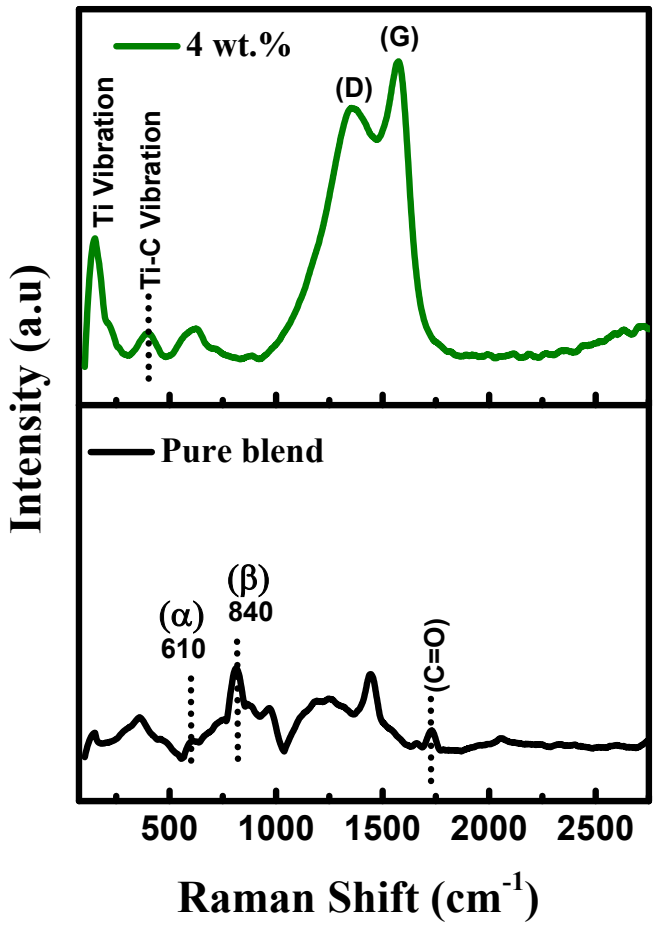

Figure S3. Raman spectra of pure blend and 4 wt.% filler loaded composite film, showing characteristic MXene vibrational modes.

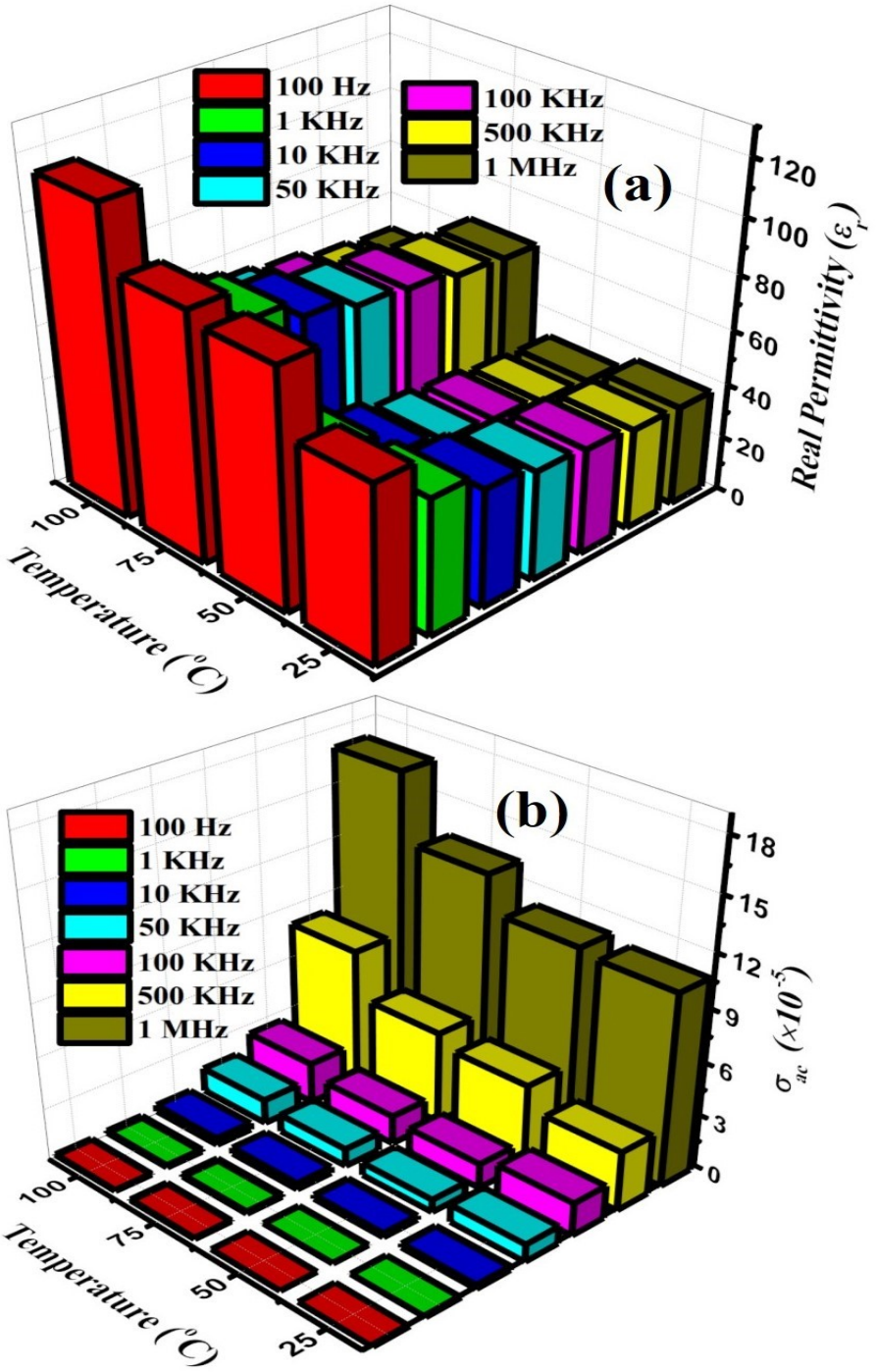

Figure S4. Temperature dependent (a) ε_r and (b) σ_{ac} at different frequency for PNC films.

Table S1. Various fitting parameters used in the Nyquist plot.

Sample Name	C_1 (F)	Q (CPE) ($F.s^{n-1}$)	n	R_1 (Ω)	C_2 (F)	R_2 (Ω)
Pure blend	1.05E-6	1.02E-8	0.89	1.98E-4	9.30E-8	1.305E-7
0.5	2.041E-6	1.73E-8	0.83	1.29E-4	2.187E-8	2.05E-6
1.0	1.481E-8	1.241E-7	0.77	1.283E-6	1.931E-7	1.551E-4
2.0	1.0915E-6	2.395E-7	0.75	1.246E-8	2.475E-8	2.421E-6
4.0	2.87E-7	1.86E-7	0.71	2.501E-5	2.854E-6	1.359E-6

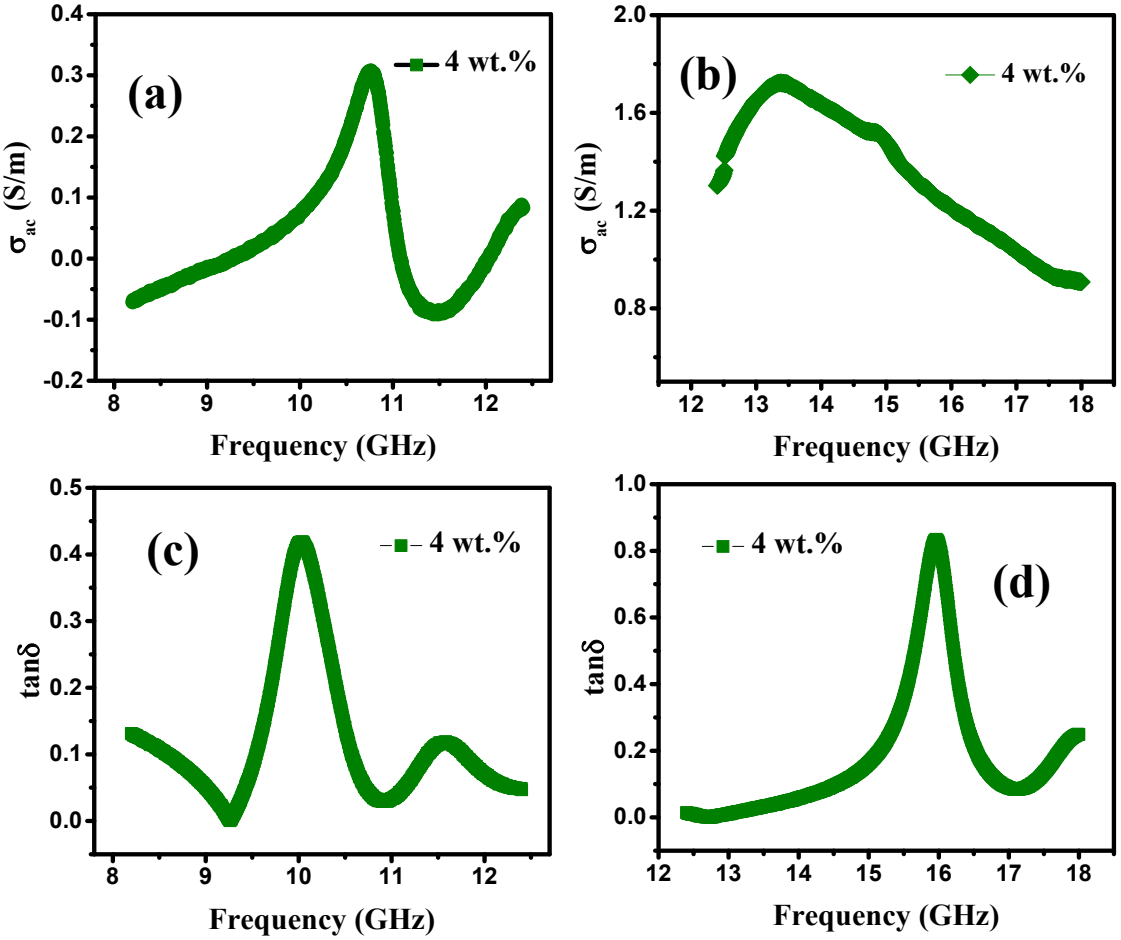

Figure S5. (a, b) AC conductivity (σ_{ac}) plots and (c, d) dielectric loss tangent (tan δ) of the 4 wt.% composite film in the X-band (8-12 GHz) and Ku-band (12-18 GHz), respectively.

Table S2. Comparison of the EMI shielding effectiveness (SE_T) of various polymer composites incorporating conductive fillers.

Polymer Matrix	Filler	Concentration	Thickness (mm)	Frequency (GHz)	SE_T (dB)	Ref.
PVDF	MWCNTs/rGO/FeCo	10 wt%	5	12	41.2	5
PVDF	Bulk $Ti_3C_2T_x$	50 wt%	1	8-12	34.49	6
PMMA	MWCNT	40 wt.%	-	50 MHz-13.5 GHz	27	7
PVDF foam	f-G	5wt.%	-	8-12	20	8
PVDF	CNT/BT-GO	3wt.%/5vol.%	1	8-18	31	9
PVDF	MWCNT	-	0.9	8-12	-8	10
PVDF	Carbonyl Fe powder	50 vol.%	1.2	8.2-12.4	20	11
PVDF	$CoFe_2O_4$ and $BaFe_2O_4$	33.33 wt.%	2	8-12	16.59 and 12.33	12
PVA	MX-$Ti_3C_2T_x$	13.9	0.025	12-18	37.1	13
PMMA wrapped PVDF/ABS	MWCNT	3	5.6	8-18	32	14
PVA	MWCNT-Graphene	10	1	1-2	32.8	15
MXene-CNT (gradient)	MXene + CNT	-	-	8-12	40	16

PVDF-HFP/PMMA	-	-	0.33	12-18	16.9	This work
PVDF-HFP/PMMA	MWCNts-MXene	4 wt.%	0.35	12-18	40.04	This work

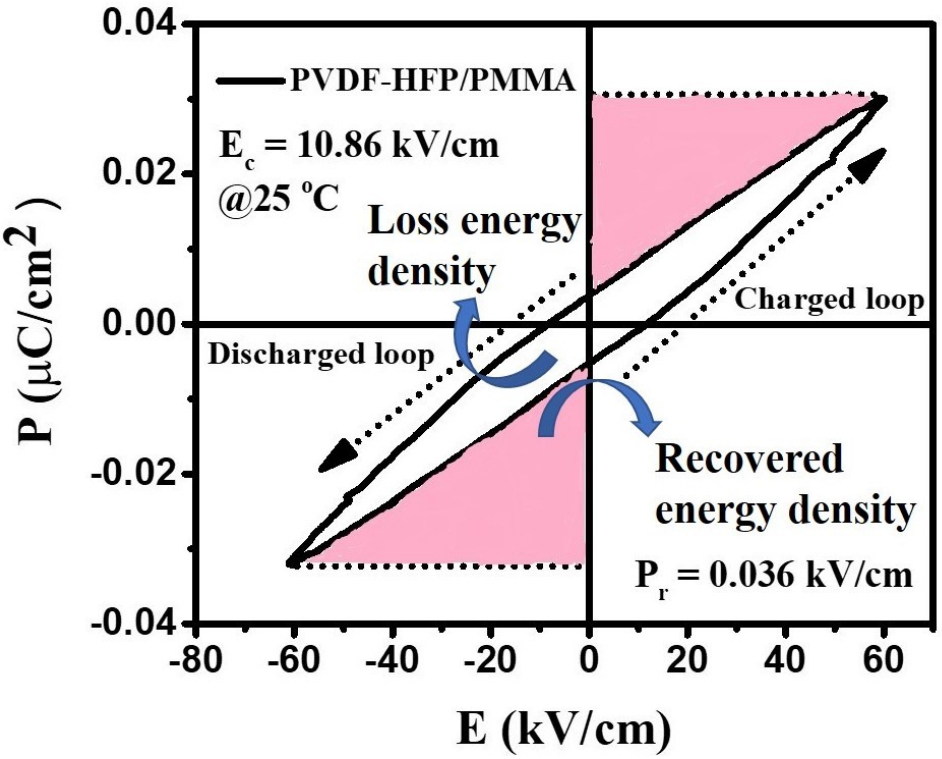

Figure S6. Charging and discharging curves of the pure PVDF-HFP/PMMA blend.

References

1. Nath, N. K., Parida, R., Parida, B. N. & Nayak, N. C. Synergistic effects of MWCNT–MXENE nanohybrids on dielectric and ferroelectric properties of PVDF/PMMA blend composites. ACS Applied Electronic Materials (2025). doi:10.1021/acsaelm.4c02179.
2. Li, Y., Zhou, X., Wang, J., Deng, Q., Li, M., Du, S., Han, Y.-H., Lee, J. & Huang, Q. Facile preparation of in situ coated Ti3C2Tx/Ni0.5Zn0.5Fe2O4composites and their electromagnetic performance. RSC Advances 7, 24698–24708 (2017).
3. Kandpal, S., Ghosh, T., Rani, C., Tanwar, M., Sharma, M., Rani, S., Pathak, D. K., Bhatia, R., Sameera, I., Jayabalan, J. & Kumar, R. Bifunctional application of Viologen-MOS2-CNT/Polythiophene device as electrochromic diode and Half-Wave rectifier. ACS Materials Au 2, 293–300 (2022).
4. Mubarak, N. M.; Yusof, F.; Alkhatib, M. F. The production of carbon nanotubes using two-stage chemical vapor deposition and their potential use in protein purification. Chemical Engineering Journal 2011, 168 (1), 461–469. https://doi.org/10.1016/j.cej.2011.01.045.
5. Arief, I., Biswas, S. & Bose, S. FeCo-Anchored Reduced Graphene Oxide Framework-Based Soft Composites Containing Carbon Nanotubes as Highly Efficient Microwave Absorbers with Excellent Heat Dissipation Ability. ACS Applied Materials & Interfaces 9, 19202–19214 (2017).
6. Rajavel, K., Luo, S., Wan, Y., Yu, X., Hu, Y., Zhu, P., Sun, R. & Wong, C. 2D Ti3C2Tx MXene/polyvinylidene fluoride (PVDF) nanocomposites for attenuation of electromagnetic radiation with excellent heat dissipation. Composites Part a Applied Science and Manufacturing 129, 105693 (2019).
7. Kim, H. M., Kim, K., Lee, C. Y., Joo, J., Cho, S. J., Yoon, H. S., Pejaković, D. A., Yoo, J. W. & Epstein, A. J. Electrical conductivity and electromagnetic interference shielding of multiwalled carbon nanotube composites containing Fe catalyst. Applied Physics Letters 84, 589–591 (2004).
8. Eswaraiah, V., Sankaranarayanan, V. & Ramaprabhu, S. Functionalized Graphene–PVDF foam composites for EMI shielding. Macromolecular Materials and Engineering 296, 894–898 (2011).

9. Sharma, M., Singh, M. P., Srivastava, C., Madras, G. & Bose, S. Poly(vinylidene fluoride)-Based Flexible and Lightweight Materials for Attenuating Microwave Radiations. ACS Applied Materials & Interfaces 6, 21151–21160 (2014).
10. Biswas, S., Arief, I., Panja, S. S. & Bose, S. Absorption-Dominated Electromagnetic Wave Suppressor Derived from Ferrite-Doped Cross-Linked Graphene Framework and Conducting Carbon. ACS Applied Materials & Interfaces 9, 3030–3039 (2016).
11. Joseph, N. & Sebastian, M. T. Electromagnetic interference shielding nature of PVDF-carbonyl iron composites. Materials Letters 90, 64–67 (2012).
12. Meena, S., Kumari, N., Gahlaut, V., Shekhar, C., Mitra, S. & Dwivedi, U. K. Electrical and EMI shielding studies of ferrite/MWCNTs/PVDF composites. Journal of Applied Polymer Science 142, (2024).
13. Jin, X., Wang, J., Dai, L., Liu, X., Li, L., Yang, Y., Cao, Y., Wang, W., Wu, H. & Guo, S. Flame-retardant poly (vinyl alcohol)/MXene multilayered films with outstanding electromagnetic interference shielding and thermal conductive performances. Chemical Engineering Journal 380, 122475 (2019).
14. Kar, G.P., Biswas, S., Bose, S., 2015. Simultaneous enhancement in mechanical strength, electrical conductivity, and electromagnetic shielding properties in PVDF–ABS blends containing PMMA wrapped multiwall carbon nanotubes. Physical Chemistry Chemical Physics 17, 14856–14865. https://doi.org/10.1039/c5cp01452b.
15. Lin, J.-H., Lin, Z.-I., Pan, Y.-J., Huang, C.-L., Chen, C.-K., Lou, C.-W., 2015. Polymer composites made of multi-walled carbon nanotubes and graphene nano-sheets: Effects of sandwich structures on their electromagnetic interference shielding effectiveness. Composites Part B Engineering 89, 424–431. https://doi.org/10.1016/j.compositesb.2015.11.014
16. Jang, J.M., Kim, J.H., Lee, J., Hong, J., Kim, D.W., Kim, S.J., 2024. Gradient-structured MXene/ZIF/CNT hybrid films for largely enhanced electromagnetic absorption in EMI shielding. Chemical Engineering Journal 503, 158691. https://doi.org/10.1016/j.cej.2024.158691